Scattering of light by polydisperse, randomly oriented, finite circular cylinders

Michael I. Mishchenko, Larry D. Travis, and Andreas Macke

We use the *T*-matrix method, as described by Mishchenko [Appl. Opt. **32,** 4652 (1993)], to compute rigorously light scattering by finite circular cylinders in random orientation. First we discuss numerical aspects of *T*-matrix computations specific for finite cylinders and present results of benchmark computations for a simple cylinder model. Then we report results of extensive computations for polydisperse, randomly oriented cylinders with a refractive index of $1.53 + 0.008i$, diameter-to-length ratios of 1/2, 1/1.4, 1, 1.4, and 2, and effective size parameters ranging from 0 to 25. These computations parallel our recent study of light scattering by polydisperse, randomly oriented spheroids and are used to compare scattering properties of the two classes of simple convex particles. Despite the significant difference in shape between the two particle types (entirely smooth surface for spheroids and sharp rectangular edges for cylinders), the comparison shows rather small differences in the integral photometric characteristics (total optical cross sections, single-scattering albedo, and asymmetry parameter of the phase function) and the phase function. The general patterns of the other elements of the scattering matrix for cylinders and aspect-ratio-equivalent spheroids are also qualitatively similar, although noticeable quantitative differences can be found in some particular cases. In general, cylinders demonstrate much less shape dependence of the elements of the scattering matrix than do spheroids. Our computations show that, like spheroids and bispheres, cylinders with surface-equivalent radii smaller than a wavelength can strongly depolarize backscattered light, thus suggesting that backscattering depolarization for nonspherical particles cannot be universally explained by using only geometric-optics considerations.

Key words: Light scattering, nonspherical particles, depolarization, aerosols, remote sensing.

1. Introduction

In several recent papers we have described the results of an extensive study of single light scattering by polydisperse, randomly oriented spheroids.[1–4] In our calculations we used a rigorous and highly efficient method, based on Waterman's *T*-matrix approach,[5] and an analytical procedure for averaging the optical cross sections and the elements of the Stokes scattering matrix of a nonspherical particle over the uniform distribution of particle orientations.[1,6] This method is especially well suited to the computation of light scattering by rotationally symmetric particles, which has been the primary motivation for choosing spheroids for that study. Also, because of its high efficiency, the method has enabled us to compute scattering properties of polydisperse rather than monodisperse spheroids. As emphasized in Refs. 1–4 and 7–9, averaging over sizes not only provides more realistic modeling of natural particle ensembles but also washes out the interference structure and ripple inherent in scattering patterns for monodisperse particles, thus permitting meaningful conclusions about the effect of particle shape, size, and refractive index on light scattering.

Another class of rotationally symmetric nonspherical particles that can be efficiently studied by using our computational method are finite circular cylinders. Unlike spheroids, the surface of finite cylinders is not completely smooth but is rather characterized by sharp, rectangular edges (Fig. 1). These edges make cylinders less regular nonspherical particles than spheroids and might well be expected to have an effect on light-scattering characteristics.[10,11] Therefore, it is the aim of this paper to perform a study of light scattering by poly-

M. I. Mishchenko and L. D. Travis are with the NASA Goddard Institute for Space Studies, 2880 Broadway, New York, New York 10025. A. Macke is with the Department of Applied Physics, Columbia University, 2880 Broadway, New York, New York 10025.

Received 26 September 1995; revised manuscript received 16 February 1996.

0003-6935/96/244927-14$10.00/0

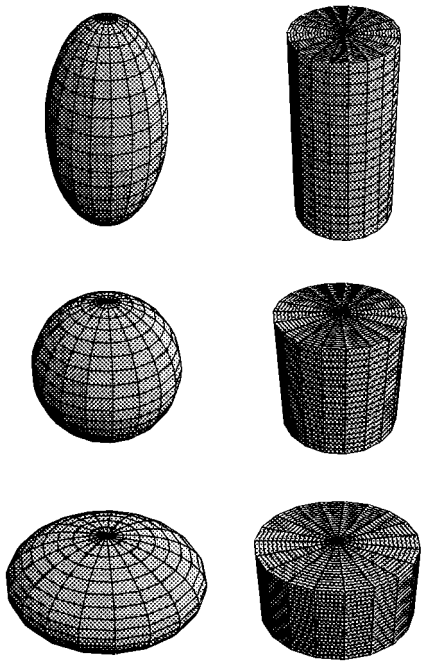

Fig. 1. Comparison of the shape of spheroids and finite circular cylinders with horizontal-to-vertical dimension ratios of 1/2 (prolate particles), 1 (compact particles), and 2 (oblate particles).

disperse, randomly oriented, finite cylinders that is analogous to that accomplished earlier for spheroids and to report those results here.[1–4] In Section 2 we briefly introduce the necessary terminology, discuss numerical aspects specific for finite cylinders, and present results of benchmark computations for a simple cylinder model. In Section 3, detailed characteristics derived from extensive computations of light scattering by polydisperse, randomly oriented, finite cylinders are reported. These results are compared with those for surface-equivalent spheres and randomly oriented spheroids, and the effect of particle shape on light scattering is discussed.

2. Numerical Aspects and Benchmark Results

The basic quantities that fully describe single scattering of light by a small-volume element comprising polydisperse, rotationally symmetric, randomly oriented particles are the ensemble-averaged extinction, C_{ext}, and scattering, C_{sca}, cross sections per particle, and the elements of the Stokes scattering matrix having the well-known block-diagonal structure[12–14]:

$$\mathbf{F}(\Theta) = \begin{bmatrix} F_{11}(\Theta) & F_{21}(\Theta) & 0 & 0 \\ F_{21}(\Theta) & F_{22}(\Theta) & 0 & 0 \\ 0 & 0 & F_{33}(\Theta) & F_{34}(\Theta) \\ 0 & 0 & -F_{34}(\Theta) & F_{44}(\Theta) \end{bmatrix}. \quad (1)$$

Here, $\Theta \in [0°, 180°]$ is the scattering angle, and the (1, 1) element (i.e., the phase function) satisfies the normalization condition

$$\frac{1}{4\pi}\int_{4\pi} d\Omega\, F_{11}(\Theta) = 1. \quad (2)$$

We have used the following method to compute these quantities for polydisperse, randomly oriented finite cylinders (for more details, see Refs. 1 and 15). The first step was to calculate the T matrix of a cylinder with respect to the spherical coordinate system with the z axis along the axis of cylinder symmetry. The accuracy parameter Δ, as defined by Eqs. (18) and (21) of Ref. 1, was set at 0.001. Then this T matrix was used in an analytical procedure to compute the orientationally averaged optical cross sections and the expansion coefficients appearing in the following expansions of the elements of the scattering matrix[16,17]:

$$F_{11}(\Theta) = \sum_{s=0}^{s_{\max}} \alpha_1{}^s P_{00}{}^s(\cos\Theta), \quad (3)$$

$$F_{22}(\Theta) + F_{33}(\Theta) = \sum_{s=2}^{s_{\max}} (\alpha_2{}^s + \alpha_3{}^s) P_{22}{}^s(\cos\Theta), \quad (4)$$

$$F_{22}(\Theta) - F_{33}(\Theta) = \sum_{s=2}^{s_{\max}} (\alpha_2{}^s - \alpha_3{}^s) P_{2,-2}{}^s(\cos\Theta), \quad (5)$$

$$F_{44}(\Theta) = \sum_{s=0}^{s_{\max}} \alpha_4{}^s P_{00}{}^s(\cos\Theta), \quad (6)$$

$$F_{21}(\Theta) = \sum_{s=2}^{s_{\max}} \beta_1{}^s P_{02}{}^s(\cos\Theta), \quad (7)$$

$$F_{34}(\Theta) = \sum_{s=2}^{s_{\max}} \beta_2{}^s P_{02}{}^s(\cos\Theta), \quad (8)$$

where $P_{mn}{}^s(x)$ are generalized spherical functions.[16,18] Because the number of numerically significant expansion coefficients, $s_{\max}$, is usually small and because the generalized spherical functions can be easily computed for essentially any number of scattering angles, the expansions of Eqs. (3)–(8) serve as a convenient and compact representation of the scattering matrix. The optical cross sections and the expansion coefficients were computed for cylinders with equal-surface-area-sphere size parameters x ranging from 0.05 to 40 with a step size of 0.05. This step size was found to be small enough to provide sufficient accuracy in computations for intermediate size parameters that used straightforward spline interpolation. The precomputed monodisperse cross sections and expansion coefficients along with spline interpolation and numerical Gauss integration were then used to average the optical cross sections and the expansion coefficients over a modified power-law size distribution given by

$$n(x) = \begin{cases} C & \text{for } x \le x_1 \\ C(x_1/x)^3 & \text{for } x_1 \le x \le x_2, \\ 0 & \text{for } x \ge x_2, \end{cases} \quad (9)$$

where $n(x)\mathrm{d}x$ is the fraction of particles with size parameters between x and $x + \mathrm{d}x$, and C is a normalization constant such that

$$\int_0^\infty \mathrm{d}x\, n(x) = 1. \tag{10}$$

Formal parameters x_1 and x_2 were chosen such that effective variance v_{eff} was fixed at 0.1, thus corresponding to a moderately wide size distribution, while effective size parameter x_{eff} varied from 0.25 to 25 in steps of 0.25. The effective size parameter and effective variance of a size distribution are defined as[13]

$$x_{\mathrm{eff}} = \frac{1}{G}\int_0^\infty \mathrm{d}x\, \pi x^3 n(x), \tag{11}$$

$$v_{\mathrm{eff}} = \frac{1}{G x_{\mathrm{eff}}^2}\int_0^\infty \mathrm{d}x (x - x_{\mathrm{eff}})^2 \pi x^2 n(x), \tag{12}$$

where

$$G = \int_0^\infty \mathrm{d}x\, \pi x^2 n(x), \tag{13}$$

and they have been shown by Hansen and Travis[13] and Mishchenko and Travis[3] to be the parameters that best characterize essentially any plausible size distribution of spherical as well as nonspherical particles in the context of light-scattering behavior. We found that, because of the absence of a sharp drop to zero at $x = x_1$, the modified power-law distribution used here provides a smoother behavior of the scattering patterns than the standard power-law distribution[13] used in our previous papers on polydisperse spheroidal scattering.[1–3] Finally, the size-averaged expansion coefficients for the 100 effective size parameters $x_{\mathrm{eff}} = 0.25(0.25)25$ were used to compute the elements of the scattering matrix for 181 scattering angles from 0° to 180° in steps of 1°. In all of our computations, the refractive index was fixed at $1.53 + 0.008i$. This value is typical of dustlike tropospheric aerosols at visible wavelengths[19] and is equal or close to that used in previous detailed studies of light scattering by Chebyshev particles,[8,20] spheroids,[1–4] and bispheres.[21] These extensive computations were repeated for five cylindrical shapes with diameter-to-length ratios of $D/L = 1/2$, 1/1.4, 1, 1.4, and 2 and were used to create color contour diagrams of the elements of the scattering matrix versus scattering angle and effective size parameter and linear plots of the optical cross sections versus effective size parameter. These results are discussed in Section 3.

The computation of the T matrix for a rotationally symmetric particle involves the numerical evaluation of integrals over zenith angle on the interval $[0, \pi]$ [see equations (39a)–(39d) on pp. 187 and 188 of Ref. 22] by using a Gaussian quadrature formula. For particles such as spheroids and finite cylinders with a plane of symmetry perpendicular to the axis of rotation, the integrals over the interval $[0, \pi]$ can be reduced to integrals over the interval $[0, \pi/2]$. However, unlike spheroids, the shape of a finite cylinder is not entirely smooth and the use of a single Gaussian quadrature on the whole interval $[0, \pi/2]$ gives poor accuracy. We have found that much better results can be obtained by dividing the interval $[0, \pi/2]$ into two subintervals $[0, \arctan(D/L)]$ and $[\arctan(D/L), \pi/2]$ and by applying separate Gaussian quadrature formulas to each of the two subintervals. This simple approach substantially improves the accuracy of the T-matrix computations and permits convergent results for cylinders with significantly larger size parameters. We have also found that an even further increase of the maximum convergent size parameter by a factor of 2–2.5 can be achieved by using extended-precision rather than double-precision floating-point computer variables, as described in Ref. 23. As a consequence, we are able to reach relatively large size parameters, as demonstrated in Fig. 2, which shows the elements of the scattering matrix for randomly oriented monodisperse cylinders with a diameter-to-length ratio of 1 and an equal-surface-area-sphere size parameter of 70. Note that the computation of Fig. 2 took 6.5 h of CPU time on an IBM reduced instruction set computer (RISC) Model 37T workstation.

We have checked our computer code for calculating light scattering by finite circular cylinders in fixed and random orientations in several ways. First, we have found that computations of the amplitude scattering matrix satisfy the general reciprocity relation[4,12,24] with high accuracy. Second, we have checked our computations for randomly oriented finite cylinders versus numerical data[10] obtained with an independent T-matrix code that employed the standard numerical averaging over orientations and double-precision floating-point variables.[25] We have compared numerical data for monodisperse cylinders with an equal-surface-area-sphere size parameter of 3, a refractive index of $1.53 + 0.006i$, and diameter-to-length ratios of 1, 2/3, 1/2, and 1/3. In most cases, the agreement in the expansion coefficients appearing in Eqs. (3)–(8) was within ± 0.0002. Third, we have found that our computations of the elements of the scattering matrix for randomly oriented cylinders are in full agreement with the general equalities[3,12,26,27] $F_{12}(0) = F_{12}(\pi) = F_{34}(0) = F_{34}(\pi) = 0$, $F_{22}(0) = F_{33}(0)$, $F_{22}(\pi) = -F_{33}(\pi)$, $F_{11}(\pi) - F_{22}(\pi) = F_{44}(\pi) - F_{33}(\pi)$, and $F_{11}(0) - F_{22}(0) = F_{33}(0) - F_{44}(0)$, as well as with general inequalities for the elements of the scattering matrix[28,29] and for the expansion coefficients appearing in the expansions of Eqs. (3)–(8).[30] The fourth test was suggested by the fact that for nonabsorbing particles (imaginary part of the refractive index equal to zero) the scattering and extinction cross sections must be equal, which our T-matrix code reproduces with high accuracy. Finally, our computations of the optical cross sections and the phase function for randomly

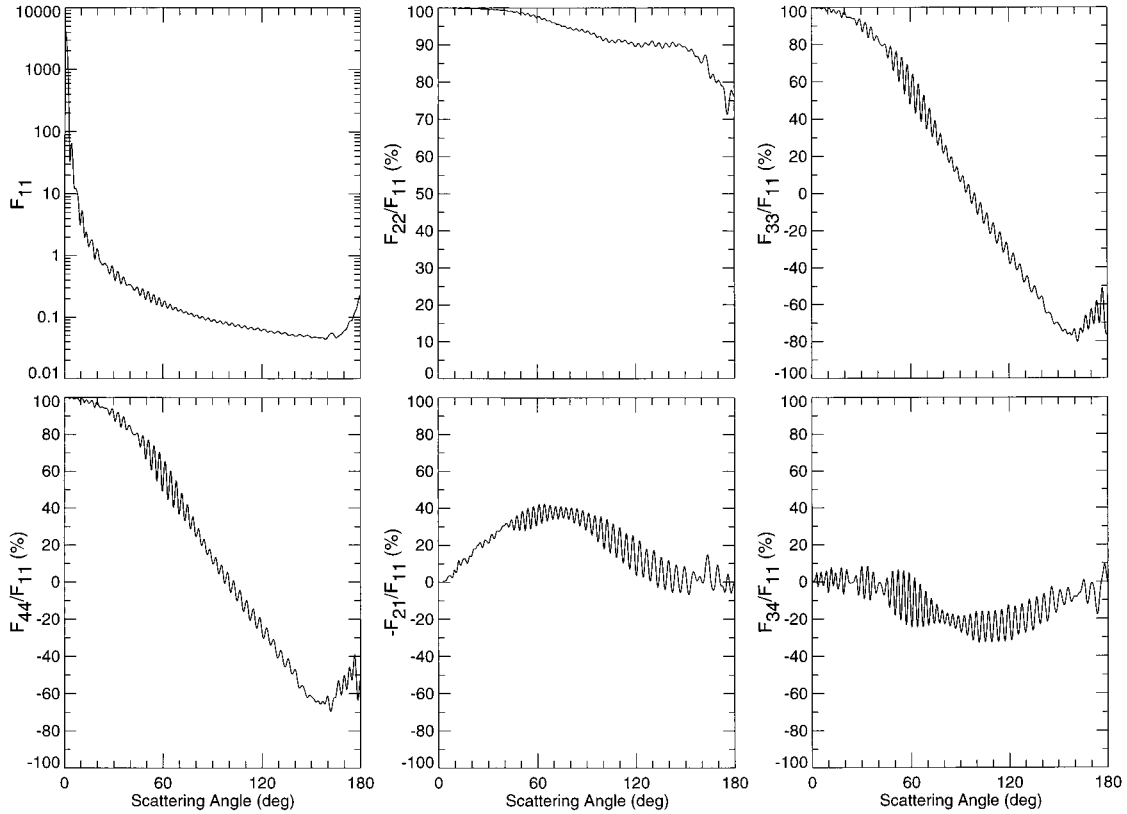

Fig. 2. Elements of the scattering matrix versus scattering angle Θ for randomly oriented, monodisperse cylinders with a diameter-to-length ratio of 1, an equal-surface-area-sphere size parameter of 70, and a refractive index of $1.53 + 0.008i$.

oriented cylinders with $D/L = 1$, surface-equivalent-sphere size parameter $x = 75$, and refractive index $1.394 + 0.00685i$ have shown excellent agreement with results of ray-tracing calculations (cf. Ref. 31).

Because most numerical methods for computing nonspherical scattering are complicated and time consuming, especially for randomly oriented particles, there is a practical need for accurate numbers in order to check the accuracy of the corresponding computer codes. Some benchmark results have already been published for randomly oriented spheroids, Chebyshev particles, and bispheres with touching and separated components.[6,15,32,33] To the best of our knowledge, no such results have been published in digital form for randomly oriented finite cylinders. We believe that, because of the high accuracy of our method reinforced by the use of extended-precision floating-point variables, our computer code is quite suitable for obtaining numbers accurate enough to serve as a benchmark. Therefore, we present in Tables 1 and 2 the expansion coefficients and the elements of the scattering matrix for a simple model of

Table 1. Expansion Coefficients from Eqs. (3)–(8) for Randomly Oriented, Monodisperse, Prolate Cylinders[a]

s	α_1^s	α_2^s	α_3^s	α_4^s	β_1^s	β_2^s
0	1.00000	0.00000	0.00000	0.91444	0.00000	0.00000
1	2.12700	0.00000	0.00000	2.19933	0.00000	0.00000
2	2.34519	3.82053	3.61229	2.26064	0.04799	−0.07636
3	1.84205	2.64563	2.68023	1.85961	0.13754	−0.22903
4	1.24783	1.73978	1.71411	1.26120	0.22472	−0.14598
5	0.70245	0.96265	0.92810	0.70368	0.17209	−0.06196
6	0.35272	0.47618	0.45319	0.34921	0.09103	−0.03782
7	0.13784	0.18852	0.17917	0.13724	0.05506	−0.02318
8	0.04653	0.06405	0.05742	0.04424	0.02485	−0.00689
9	0.01197	0.01652	0.01364	0.01061	0.00840	−0.00193
10	0.00256	0.00351	0.00257	0.00203	0.00209	−0.00031
11	0.00044	0.00060	0.00038	0.00031	0.00040	−0.00004
12	0.00006	0.00008	0.00005	0.00004	0.00006	0.00000

[a]Cylinders have a diameter-to-length ratio of 1/2, an equal-surface-area-sphere size parameter of 3, and a refractive index of $1.53 + 0.008i$.

Table 2. Elements of the Scattering Matrix Versus Scattering Angle Θ for Randomly Oriented, Monodisperse, Prolate Cylinders[a]

Θ (deg)	F_{11}	F_{22}	F_{33}	F_{44}	F_{21}	F_{34}
0	9.81664	9.77960	9.77960	9.74256	0.00000	0.00000
10	8.99021	8.95155	8.95115	8.91869	−0.07119	0.03889
20	6.93400	6.89084	6.88596	6.86619	−0.21421	0.12579
30	4.57199	4.52257	4.50638	4.50453	−0.29964	0.20075
40	2.66452	2.60869	2.57988	2.59729	−0.27277	0.22610
50	1.45651	1.39574	1.36086	1.39494	−0.17657	0.20475
60	0.80457	0.74147	0.70836	0.75365	−0.07692	0.15849
70	0.47165	0.40924	0.38126	0.43128	−0.00699	0.10376
80	0.29492	0.23598	0.21101	0.26015	0.02915	0.04839
90	0.19722	0.14418	0.11514	0.15955	0.03667	−0.00067
100	0.14492	0.09995	0.05608	0.09334	0.02421	−0.03507
110	0.11928	0.08433	0.01449	0.04287	0.00435	−0.04996
120	0.10797	0.08402	−0.01926	−0.00057	−0.01057	−0.04787
130	0.10471	0.08999	−0.04877	−0.03812	−0.01478	−0.03682
140	0.10898	0.09768	−0.07471	−0.06644	−0.01057	−0.02455
150	0.12261	0.10611	−0.09642	−0.08194	−0.00422	−0.01464
160	0.14394	0.11514	−0.11274	−0.08500	−0.00047	−0.00717
170	0.16451	0.12290	−0.12272	−0.08140	0.00021	−0.00197
180	0.17313	0.12605	−0.12605	−0.07898	0.00000	0.00000

[a]Cylinders have a diameter-to-length ratio of 1/2, an equal-surface-area-sphere size parameter of 3, and a refractive index of $1.53 + 0.008i$.

monodisperse, randomly oriented, finite cylinders with an equal-surface-area-sphere size parameter of 3, a diameter-to-length ratio of $D/L = 0.5$, and a refractive index of $1.53 + 0.008i$. Note that the expansion coefficients with $s > 12$ are smaller in absolute value than 5×10^{-6}. The elements of the scattering matrix are also visualized in Fig. 3. At a wavelength $\lambda = \pi/5\ \mu\text{m} \approx 0.62832\ \mu\text{m}$, the extinction cross section for this model is $C_{\text{ext}} = 0.71596\ \mu\text{m}^2$ and the scattering cross section is $C_{\text{sca}} = 0.69191\ \mu\text{m}^2$.

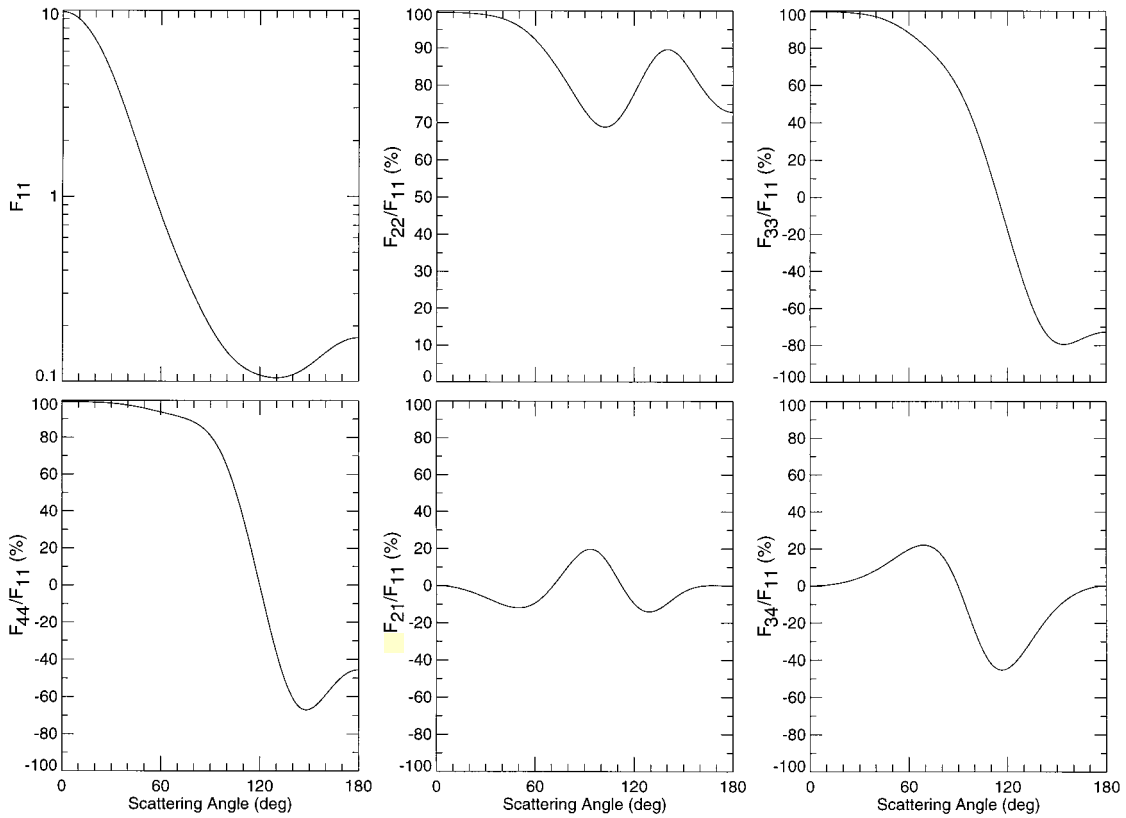

Fig. 3. Elements of the scattering matrix versus scattering angle Θ for randomly oriented, monodisperse, prolate cylinders with a diameter-to-length ratio of 1/2, an equal-surface-area-sphere size parameter of 3, and a refractive index of $1.53 + 0.008i$.

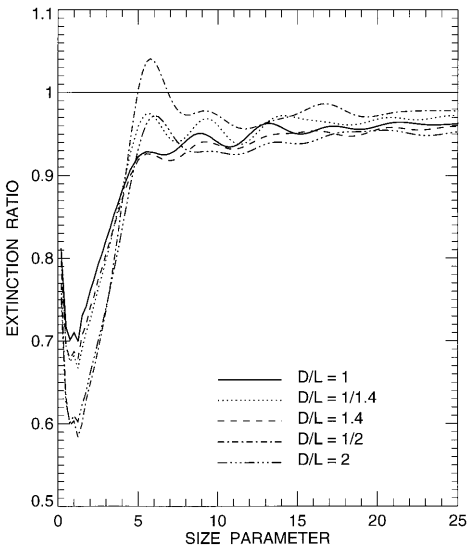

Fig. 4. Ratio of the extinction cross section for randomly oriented, polydisperse cylinders with diameter-to-length ratios $D/L = 1$, 1/1.4, 1.4, 1/2, and 2 relative to that for surface-equivalent spheres versus effective size parameter.

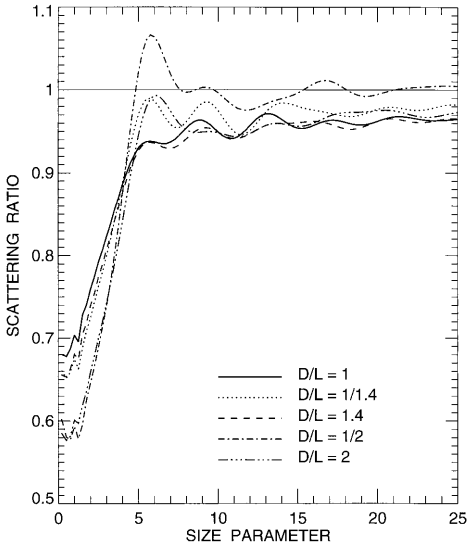

Fig. 5. Ratio of the scattering cross section for randomly oriented polydisperse cylinders relative to that for surface-equivalent spheres versus effective size parameter.

An internal convergence test suggests that the cross sections and the table entries should be accurate to within a few units in the last digits given.

3. Discussion

A. Optical Cross Sections, Single-Scattering Albedo, Asymmetry Parameter of the Phase Function, and Backscattered Fraction

For spheroids, nonspherical–spherical differences in all light-scattering characteristics tend to zero with the aspect ratio (i.e., the ratio of the larger to the smaller spheroidal axes) approaching 1[1–4] because spheroids with an aspect ratio of 1 are spherical particles. However, circular cylinders with a diameter-to-length ratio of 1 are already nonspherical particles with a shape significantly deviating from that of a sphere (the ratio of the largest to the smallest cylinder dimensions equals $2^{1/2} \approx 1.414$). Accordingly, Figs. 4–8 show that nonspherical–spherical differences in extinction C_{ext}, scattering C_{sca}, absorption C_{abs}, cross sections, single-scattering albedo ϖ, and the asymmetry parameter of the phase function $\langle \cos \Theta \rangle = \alpha_1{}^1/3$ between cylinders with $D/L = 1$ and spheres are already significant. Furthermore, the differences in C_{ext}, C_{sca}, and $\langle \cos \Theta \rangle$ do not necessarily increase with an increasing cylinder asphericity parameter defined as $\varepsilon = D/L$ for $D > L$ and $\varepsilon = L/D$ for $L > D$. In fact, at effective size parameters larger than approximately 7, nonspherical–spherical differences in the extinction and scattering cross sections and the asymmetry parameter are smaller for prolate cylinders with a diameter-to-length ratio of 1/2 than for more compact cylinders with $D/L = 1$, 1/1.4, and 1.4. However, nonspherical–spherical differences in absorption cross section C_{abs} and single-scattering albedo ϖ do increase with increasing ε. The absorption cross section systematically decreases with increasing ε, as is the case for spheroids,[3,4] whereas ϖ and $\langle \cos \Theta \rangle$ increase with increasing ε at size parameters larger than 3. We note that maximal nonspherical–spherical differences in the integral photometric characteristics occur at effective size parameters smaller than approximately 5. The same result was found for randomly oriented spheroids[3,4] and is an artifact of comparing surface-equivalent particles, whereas light-scattering characteristics of particles smaller than a wavelength depend primarily on particle volume rather than surface area.[12,14] At effective size parameters larger than approximately 10, nonspherical–spherical differences in the

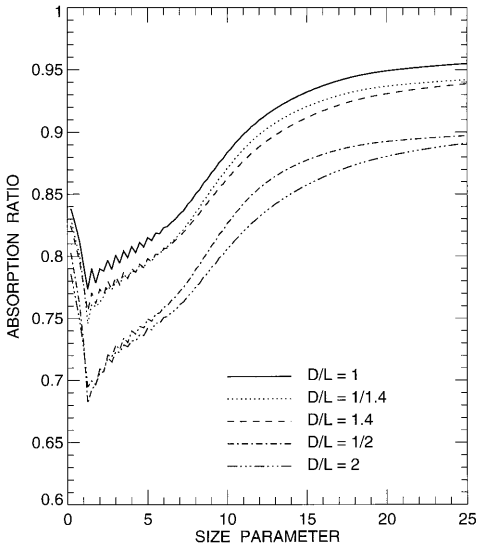

Fig. 6. Ratio of the absorption cross section for randomly oriented polydisperse cylinders relative to that for surface-equivalent spheres versus effective size parameter.

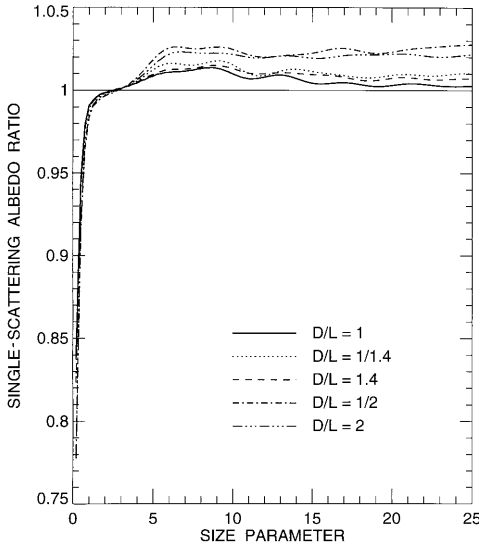

Fig. 7. Ratio of the single-scattering albedo for randomly oriented polydisperse cylinders relative to that for surface-equivalent spheres versus effective size parameter.

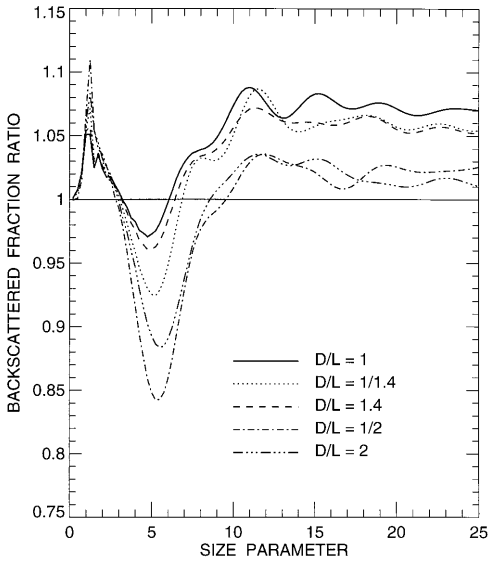

Fig. 9. Ratio of the backscattered fraction for randomly oriented polydisperse cylinders relative to that for surface-equivalent spheres versus effective size parameter.

integral photometric characteristics are relatively small, thus resembling the case for spheroids.[3,4] However, the magnitude of nonspherical–spherical differences for cylinders can be noticeably larger than that for aspect-ratio-equivalent spheroids.

The backscattered fraction for isotropically incident radiation β is defined as[34]

$$\beta = \frac{1}{2\pi}\int_0^{\pi} d\Theta F_{11}(\Theta)\Theta \sin \Theta. \tag{14}$$

This quantity enters the two-stream approximation and is sometimes used to estimate experimentally the asymmetry parameter of the phase function.[35]

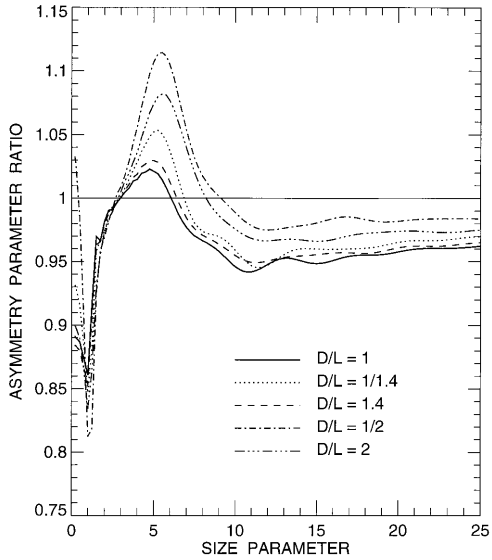

Fig. 8. Ratio of the asymmetry parameter of the phase function for randomly oriented polydisperse cylinders relative to that for surface-equivalent spheres versus effective size parameter.

Figure 9 shows the ratio β(cylinders)/β(spheres) as a function of x_{eff} and reveals that spherical–nonspherical differences in the backscattered fraction are relatively small. Interestingly, the asymmetry parameter and the backscattered fraction ratios displayed in Figs. 8 and 9 are essentially mirror images of one another with respect to the horizontal line at the level of 1, so that for each size parameter the larger the asymmetry parameter ratio the smaller the backscattered fraction ratio. This relationship was first found by Mugnai and Wiscombe[20] in their T-matrix computations for randomly oriented Chebyshev particles and then by Mishchenko *et al.*[36] in computations for polydisperse, randomly oriented spheroids.

B. Phase Function and Extinction-to-Backscatter Ratio

Figure 10 (left column, three lower diagrams) shows ratio ϱ of the phase function for polydisperse, randomly oriented cylinders relative to that for surface-equivalent spheres. The pattern of ϱ as a function of effective size parameter and scattering angle for cylinders strikingly resembles that for spheroids[3,4,36] and shows, for size parameters $\gtrsim$5, the following distinct ϱ regions in order of increasing scattering angle: (1) nonsphere $\approx$ sphere, (2) nonsphere $>$ sphere, (3) nonsphere $<$ sphere, (4) nonsphere $\gg$ sphere, (5) nonsphere $\ll$ sphere (see also Fig. 11). The only substantial difference between the ϱ patterns for spheroids and cylinders is the weak dependence of the ϱ pattern for cylinders on parameter D/L. This means that the boundaries of the five regions remain essentially fixed with a varying diameter-to-length ratio for cylinders but move significantly with changing shape for spheroids.[3,4,36]

Region 1 is the region of exact forward scattering and is least sensitive to particle nonsphericity be-

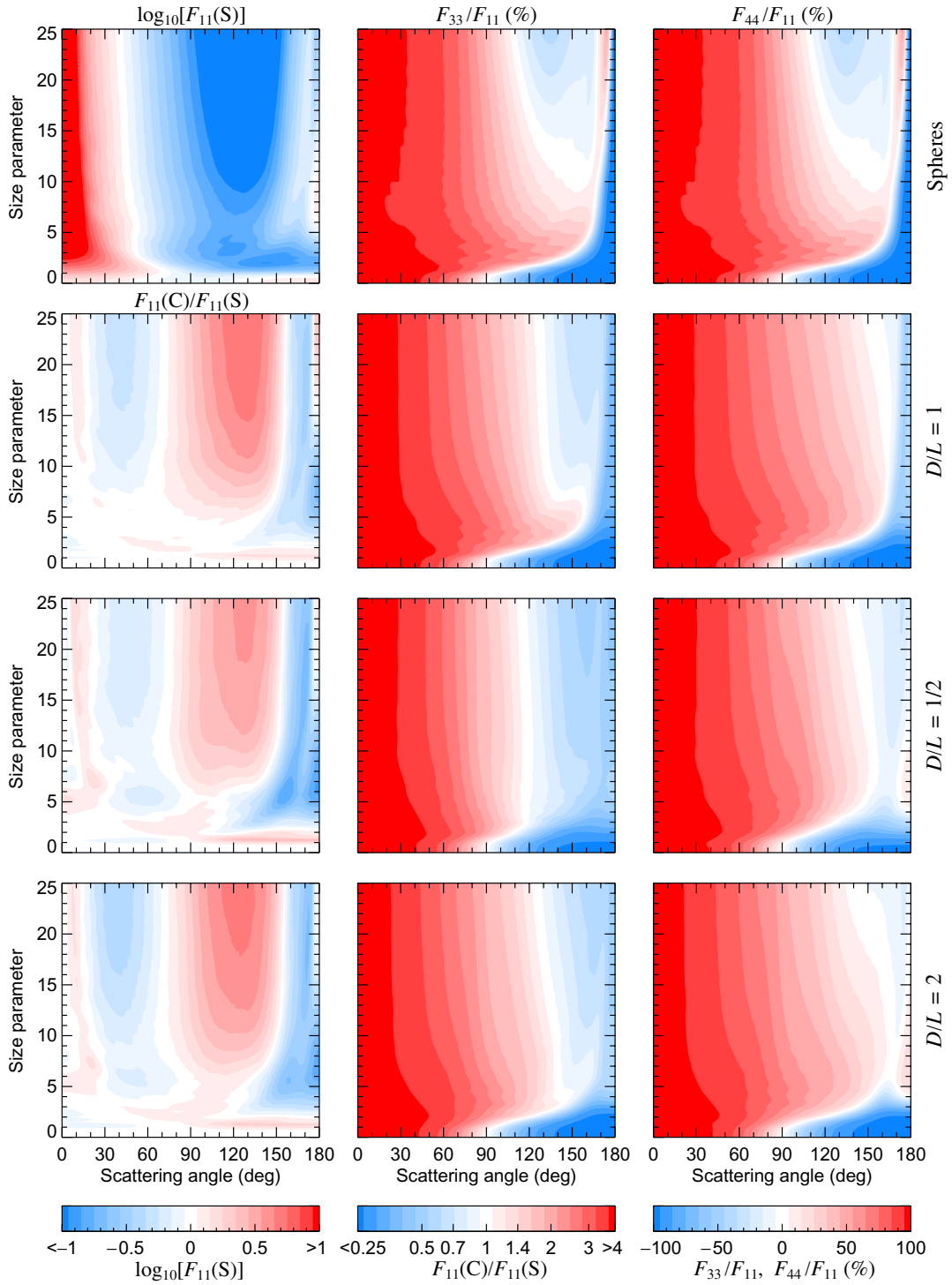

Fig. 10. Upper-left diagram shows the logarithm of the phase function versus scattering angle and effective size parameter for polydisperse spheres with a refractive index of $1.53 + 0.008i$ and an effective variance of $\nu_{\text{eff}} = 0.1$. This diagram can be quantified by using the left-hand color bar at the bottom of the figure. The three lower diagrams of the left-hand column show the ratio of the phase function for polydisperse, randomly oriented cylinders with diameter-to-length ratios $D/L = 1$, $1/2$, and 2 relative to that for surface-equivalent spheres. These diagrams can be quantified by using the middle color bar. The middle and the right-hand columns show ratios F_{33}/F_{11} and F_{44}/F_{11} of the elements of the scattering matrix for polydisperse, surface-equivalent spheres and randomly oriented cylinders. These diagrams can be quantified by using the right-hand color bar. Note that visible boundaries between discrete colors in the figures and color bars permit convenient and easy quantification of the respective diagrams by using the white color as the reference.

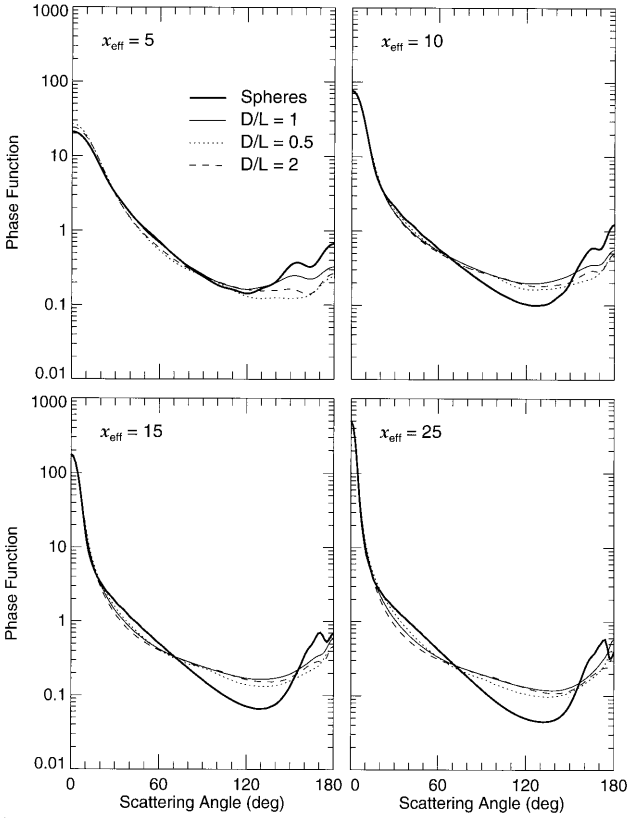

Fig. 11. Phase function versus scattering angle for polydisperse, randomly oriented cylinders and surface-equivalent spheres with effective size parameters x_{eff} = 5, 10, 15, and 25.

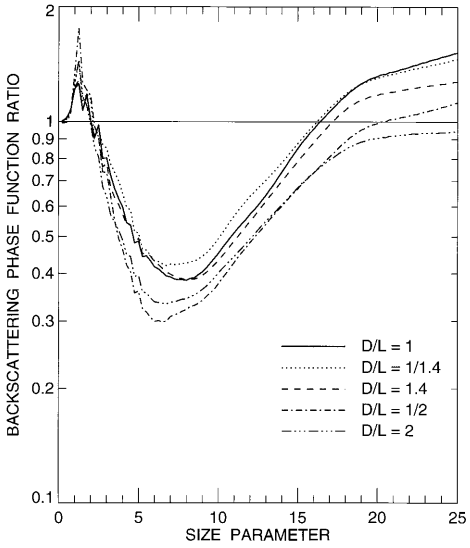

Fig. 12. Ratio of the phase function at $\Theta = 180°$ for randomly oriented polydisperse cylinders relative to that for surface-equivalent spheres versus effective size parameter.

cause of the dominant contribution of the diffraction component, which is essentially the same for surface-equivalent convex particles.[12] The second region, in which $\varrho > 1$, is the region of near-forward scattering and becomes more pronounced with increasing asphericity for both prolate and oblate cylinders, thus resembling the case for spheroids.[3,4,36] The third region, where $\varrho < 1$, extends from approximately 20° to approximately 70° and is more pronounced for oblate than for prolate cylinders, again in agreement with computations for prolate versus oblate spheroids.[3,4,36] Region 4 is the region of side scattering and extends from approximately 75° to approximately 155°. Here ratio ϱ can exceed 2.5. Although this value is smaller than that for surface-equivalent spheroids, for which ϱ can exceed 4,[3,4,36] it nonetheless indicates a strongly enhanced side scattering as opposed to a wide and deep side-scattering minimum in the phase function for spherical particles (upper left diagram of Fig. 10 and Fig. 11). Finally, region 5 is the region of near-backward scattering where values of ϱ as small as 0.3 demonstrate that another major effect of nonsphericity is to suppress the glory and rainbow features that are prominent in the phase function for spherical particles. Our computations indicate, however, that cylinders with effective size parameters larger than 16 can have larger phase function values at exactly the backscattering direction than surface-equivalent spheres. This is better illustrated in Fig. 12, which shows the ratio of the phase function at $\Theta = 180°$ for cylinders to that for surface-equivalent spheres. The only exception are oblate cylinders with a diameter-to-length ratio of 2. Because this enhanced scattering at $\Theta = 180°$ for cylinders occurs at relatively larger size parameters, it might be explained by using geometric optics considerations, specifically, double internal reflections from mutually perpendicular facets. It should be noted, however, that oblate spheroids with aspect ratios less than approximately 1.4 and size parameters larger than approximately 12 also produce greater backscattering phase function values than surface-equivalent spheres.[3,4,36]

A backscattering characteristic widely used in lidar applications[37–40] is the extinction-to-backscatter ratio, defined as

$$R_{eb} = \frac{C_{ext}}{C_{sca} P(180°)}. \tag{15}$$

This quantity is important because it enters the lidar equation[40] and has to be determined precisely to provide a high accuracy of aerosol or cloud optical thickness retrievals from lidar measurements. Mie computations for spheres show that R_{eb} is extremely sensitive to particle size and refractive index. Figure 13 demonstrates that the extinction-to-backscatter ratio is also strongly shape dependent, so that ratio R_{eb}(cylinders)/R_{eb}(spheres) can be either much larger or much smaller than 1. Obviously, these results, as well as those for spheroids,[36] strongly suggest that the effect of particle shape should be explicitly taken into account in analyzing lidar measurements for nonspherical particles. It may also be noted that laboratory measurements of light scattering at exactly the backscattering direction are ex-

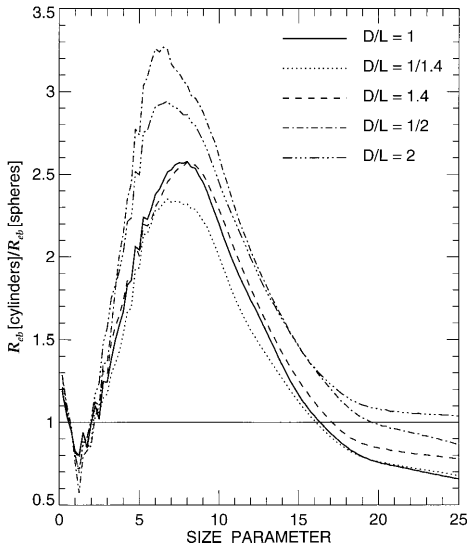

Fig. 13. Ratio of extinction-to-backscatter ratio R_{eb} for randomly oriented polydisperse cylinders relative to that for surface-equivalent spheres versus effective size parameter.

tremely difficult, if not impossible, thus greatly enhancing the value of rigorous theoretical computations for nonspherical versus spherical particles.

C. Ratio F_{22}/F_{11}

For spheroids with an aspect ratio of 1, i.e., for spheres, ratio F_{22}/F_{11} is identically equal to 1. Cylinders with a diameter-to-length ratio of 1 are already nonspherical particles and show a significant deviation of this ratio from unity (Fig. 14, left column). For all cylindrical shapes that we have studied (i.e., with $D/L = 1/2$, 1/1.4, 1, 1.4, and 2), the pattern of ratio F_{22}/F_{11} as a function of effective size parameter and scattering angle is qualitatively similar, showing side-scattering and backscattering minima separated by a vertical bridge of larger F_{22}/F_{11} values centered near 170°. The depths of the minima are, however, dependent on the diameter-to-length ratio. The side-scattering minimum is deeper for compact ($D/L = 1$) and prolate ($D/L < 1$) cylinders, whereas the depth of the back-scattering minimum increases with increasing cylinder asphericity. Ratio F_{22}/F_{11} for spheroids also shows a distinct backscattering minimum. However, unlike the case for cylinders, this minimum can become significantly deeper with the decreasing aspect ratio of prolate spheroids.[3,4] As for spheroids, ratio F_{22}/F_{11} for cylinders is nearly shape independent and close to unity at scattering angles smaller than 90° or at effective size parameters smaller than 2. A comparison of these computations with those reported in Refs. 3 and 4 suggests that, in general, cylinders show less variability in ratio F_{22}/F_{11} with shape than surface-equivalent spheroids.

D. Ratios F_{33}/F_{11} and F_{44}/F_{11}

For spheres, ratio F_{33}/F_{11} is identically equal to ratio F_{44}/F_{11} (see upper-middle and upper-right diagrams in Fig. 10) and has two negative regions at side-scattering and backscattering angles separated by a narrow positive branch for size parameters larger than approximately 10. With the increasing aspect ratio of spheroids, the side-scattering negative region weakens and ultimately disappears, while the backscattering negative region significantly widens.[3,4] Furthermore, ratios F_{33}/F_{11} and F_{44}/F_{11} become noticeably different from each other. Also for spheroids, both ratios are strongly aspect ratio dependent and are substantially different for prolate and oblate spheroids of the same aspect ratio.

Figure 10 shows that the narrow positive branch separating the side-scattering and backscattering negative regions for spheres is already absent for the least aspherical cylinders with a length-to-diameter ratio of 1 and that the shape dependence of both ratios is rather weak. As for spheroids, the region of negative F_{33}/F_{11} values is wider and deeper than that for F_{44}/F_{11}. For most scattering angles and size parameters, F_{44}/F_{11} is larger than F_{33}/F_{11}. Also, unlike ratio F_{33}/F_{11}, ratio F_{44}/F_{11} can be positive at backscattering angles. However, the shape dependence of the backscattering region of positive F_{44}/F_{11} values may represent a noticeable difference between cylinders and spheroids. Specifically, for cylinders this region becomes more pronounced with increasing ε, whereas for prolate spheroids it can become significantly weaker with an increasing aspect ratio.[3,4]

E. Linear Polarization ($-F_{21}/F_{11}$)

As discussed in Refs. 2–4 and 41, the most remarkable feature of the degree of linear polarization for polydisperse, randomly oriented spheroids is a bridge of positive polarization at scattering angles near 120° that extends upward from the region of Rayleigh scattering. This bridge was also observed by Perry *et al.*[42] in their laboratory measurements of light scattering by narrow size distributions of nearly cubically shaped NaCl particles with mean size parameters ranging from 3.1 to 19.9. Positive polarization at side-scattering angles was also found in laboratory measurements by Sassen and Liou[43] for platelike ice crystals and in measurements by Kuik[25] for irregular quartz grains. Asano and Sato[41] discussed the possible origin of positive polarization at side-scattering angles for large nonspherical particles by using geometric optics considerations.

Figure 14 (middle column) shows that randomly oriented polydisperse cylinders do not produce as pronounced a bridge of positive polarization as that found for spheroids.[2–4] Instead, prolate and oblate cylinders with $\varepsilon = 2$ produce what can be called a bridge of neutral polarization at approximately the same scattering angles, whereas aspect-ratio-equivalent spheroids produce the bridge of weak but distinctly positive polarization.[2–4] As for spheroids, one of the effects of increasing ε for cylindrical particles is to make the overall polarization more neutral and featureless. Another common effect of increasing asphericity is to extend the region of Rayleigh polarization to larger size parameters (cf. Refs. 2, 10, and 44).

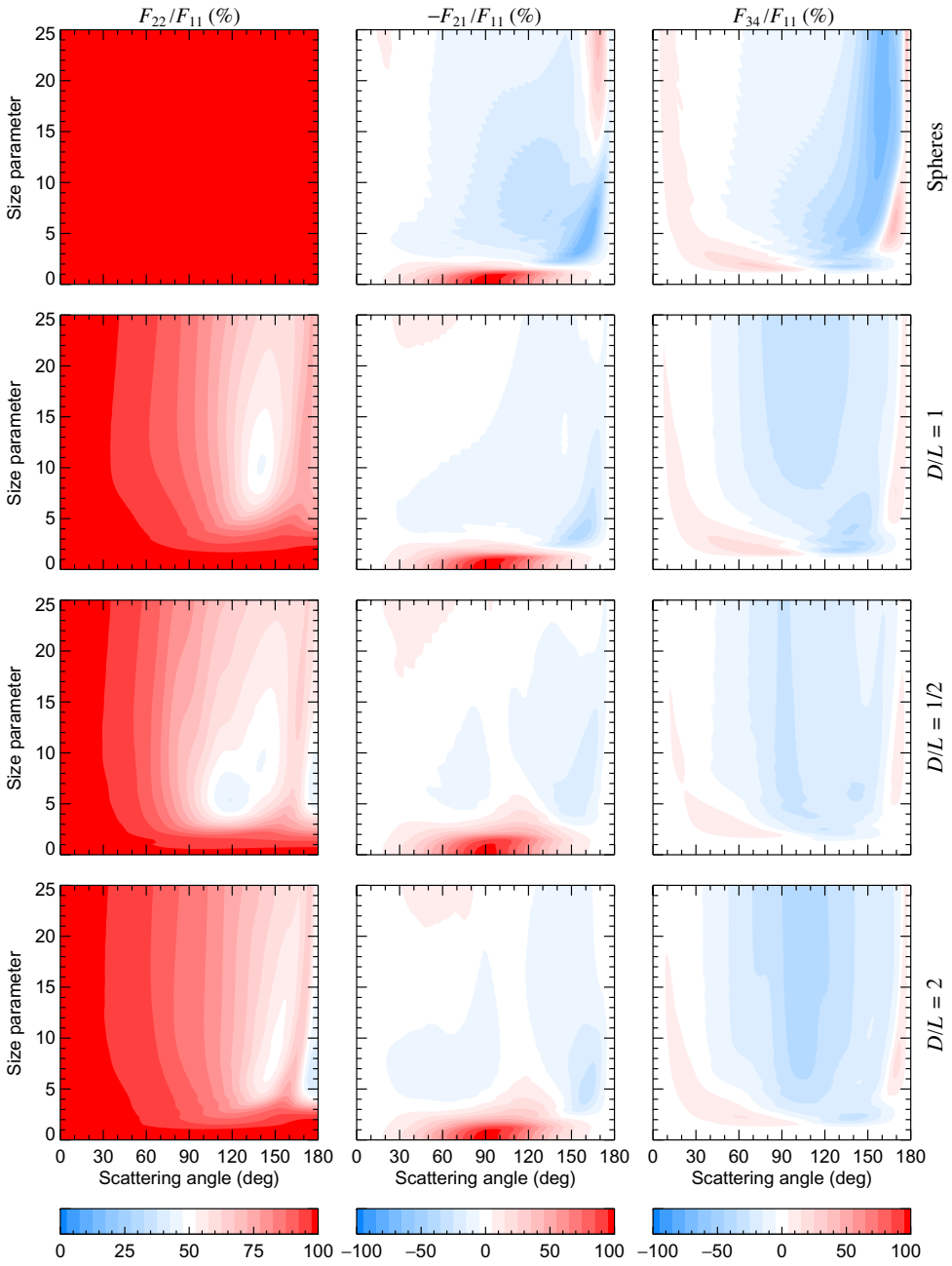

Fig. 14. Ratios F_{22}/F_{11}, $-F_{21}/F_{11}$, and F_{34}/F_{11} of the elements of the scattering matrix for polydisperse, surface-equivalent spheres and randomly oriented cylinders with diameter-to-length ratios $D/L = 1$, 1/2, and 2. The diagrams in each column should be quantified by using the color bar below this column.

F. Ratio F_{34}/F_{11}

It has been demonstrated in Refs. 3 and 4 that the general pattern of the sign of ratio F_{34}/F_{11} is the same for spheres and spheroids, with a broad side-scattering region of negative values separating two positive branches at small and large scattering angles. Figure 14 (right column) suggests that this general pattern is also typical of polydisperse, randomly oriented cylinders. However, cylinders show less variability of ratio F_{34}/F_{11} with particle shape than do spheroids. The forward-scattering region seems to be especially shape independent, thus rendering possible the use of Mie theory at small scattering angles for sizing nonspherical particles. This conclusion is in full agreement with the results of the above-mentioned laboratory measurements of Perry *et al.*[42] for wavelength-sized salt particles.

G. Backscattering Depolarization Ratios

Two scattering characteristics that are often considered sensitive indicators of particle nonsphericity are the linear, δ_L, and circular, δ_C, backscattering depo-

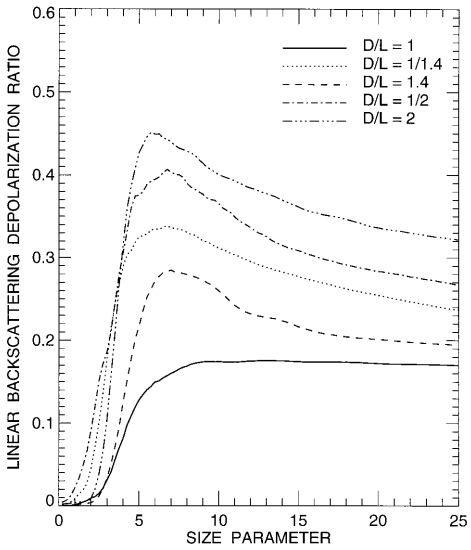

Fig. 15. Linear backscattering depolarization ratio versus effective size parameter for randomly oriented polydisperse cylinders.

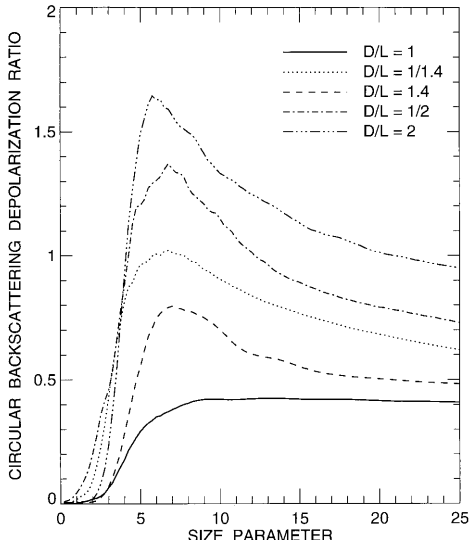

Fig. 16. Circular backscattering depolarization ratio versus effective size parameter for randomly oriented polydisperse cylinders.

larization ratios,[45–48] defined as

$$\delta_L = \frac{F_{11}(180°) - F_{22}(180°)}{F_{11}(180°) + F_{22}(180°)}, \tag{16}$$

$$\delta_C = \frac{F_{11}(180°) + F_{44}(180°)}{F_{11}(180°) - F_{44}(180°)}. \tag{17}$$

For spherical particles, $F_{22}(180°) \equiv F_{11}(180°)$ and $F_{44}(180°) \equiv -F_{11}(180°)$ and, as a consequence, both ratios vanish. For nonspherical particles these identities do not generally hold, thus causing nonzero backscattering depolarization ratios. Figures 15 and 16 show δ_L and δ_C computed for polydisperse, randomly oriented polydisperse cylinders. Note that for any randomly oriented particles having a plane of symmetry, the linear and circular backscattering depolarization ratios are not independent of each other but rather obey relationship[27]

$$\delta_C = \frac{2\delta_L}{1 - \delta_L}. \tag{18}$$

It is seen that for prolate as well as for oblate spheroids both δ_L and δ_C substantially deviate from zero, thus illustrating their usefulness as indicators of nonsphericity. Previous calculations for spheroids reported in Refs. 3, 4, and 27 have shown that the backscattering depolarization ratios cannot be considered unambiguous indicators of the degree of the departure of particle shape from that of a sphere, because nearly spherically shaped spheroids can be stronger depolarizers than spheroids with much larger aspect ratios. Interestingly, however, our computations displayed in Figs. 15 and 16 show that for size parameters larger than approximately 3, both δ_L and δ_C increase with increasing ε for prolate as well as for oblate cylinders.

Figures 15 and 16 do demonstrate (also see Plate 1 of Ref. 27) that large and even maximum depolarization values can be reached at size parameters smaller than 6, i.e., for particles with equivalent-sphere radii smaller than the wavelength of the incident light. At such small size parameters the traditional geometric optics concepts of rays, refractions, and reflections become physically meaningless[12] and cannot be used to explain the mechanism of backscattering depolarization. Furthermore, geometric optics completely fails to explain the strong and complicated size parameter dependence of the depolarization ratios as demonstrated, e.g., by Plate 1 of Ref. 27. Indeed, the geometric optics explanation in terms of multiple internal reflections[49,50] implies that δ_L and δ_C are size parameter independent for nonabsorbing particles and should monotonically decrease with increasing size parameter for absorbing particles. This is just the opposite of what is seen in Fig. 6 of Ref. 4, Plate 1 of Ref. 27, Fig. 13 of Ref. 41, and Figs. 15 and 16 of this paper. It thus appears that multiple internal reflections in nonspherical particles, as discussed in Refs. 49 and 50, cannot be considered the universal explanation of backscattering depolarization. It may well be that the only explanation of backscattering depolarization for small nonspherical particles is the lack of spherical symmetry that affects rigorous numerical solutions of Maxwell's equations by means of corresponding boundary conditions.

4. Summary and Conclusions

In this paper we have used the *T*-matrix method, as described in Refs. 1, 6, and 23, to compute light scattering by finite circular cylinders in random orientation. First we briefly described the computational scheme for calculating polydisperse optical cross sections and elements of the scattering matrix, discussed numerical aspects of *T*-matrix computations specific for finite cylinders, and presented results of benchmark computations for a simple cylinder model

that can be used for checking other rigorous or approximate methods for computing nonspherical scattering. Then we reported results of extensive computer calculations for polydisperse, randomly oriented cylinders with diameter-to-length ratios ranging from 1/2 to 2 and a refractive index close to that of dustlike tropospheric aerosols at visible wavelengths. These calculations parallel our recent studies of light scattering by polydisperse, randomly oriented spheroids[1–4,36] and were used to compare scattering properties of the two classes of simple convex particles.

Despite the large shape difference between the two particle types (completely smooth surface for spheroids and sharp rectangular edges for cylinders), the comparison reveals relatively small differences in the integral photometric characteristics (total optical cross sections, single-scattering albedo, and asymmetry parameter of the phase function) and the phase function. Like spheroids, cylinders exhibit enhanced scattering at middle angles and suppressed scattering at near-backward directions in comparison with phase functions for surface-equivalent spheres. This result supports the conclusion of Refs. 36 and 51 that nonsphericity of dustlike tropospheric aerosols should be explicitly taken into account in retrieving aerosol optical thickness from satellite lidar or reflectance measurements. The general patterns of the other elements of the scattering matrix for cylinders and aspect-ratio-equivalent spheroids are also qualitatively similar, although significant quantitative differences can be found in some particular cases. In general, cylinders show much less variability of the elements of the scattering matrix with shape than spheroids.

An important result of our computations is that, like small spheroids and bispheres, cylinders with surface-equivalent radii less than a wavelength can strongly depolarize backscattered light. This result shows the weakness of explanations of backscattering depolarization for nonspherical particles based solely on geometric optics considerations.

We are grateful to W. M. F. Wauben for sending us numerical data for randomly oriented cylinders that were used for checking the accuracy of our *T*-matrix code. This research was supported by the NASA Earth Observing System Project in providing for the Earth Observing Scanning Polarimeter instrument and analysis algorithm development and by the NASA First International Satellite Cloud Climatology Project Regional Experiment III Project.

References

1. M. I. Mishchenko, "Light scattering by size-shape distributions of randomly oriented axially symmetric particles of a size comparable to a wavelength," Appl. Opt. **32,** 4652–4666 (1993).
2. M. I. Mishchenko and L. D. Travis, "Light scattering by polydisperse, rotationally symmetric nonspherical particles: linear polarization," J. Quant. Spectrosc. Radiat. Transfer **51,** 759–778 (1994).
3. M. I. Mishchenko and L. D. Travis, "Light scattering by polydispersions of randomly oriented spheroids with sizes comparable to wavelengths of observation," Appl. Opt. **33,** 7206–7225 (1994).
4. M. I. Mishchenko, L. D. Travis, and D. W. Mackowski, "*T*-matrix computations of light scattering by nonspherical particles: a review," J. Quant. Spectrosc. Radiat. Transfer **55,** 535–575 (1996).
5. P. C. Waterman, "Symmetry, unitarity, and geometry in electromagnetic scattering," Phys. Rev. D **3,** 825–839 (1971).
6. M. I. Mishchenko, "Light scattering by randomly oriented axially symmetric particles," J. Opt. Soc. Am. A **8,** 871–882 (1991); "Erratum," **9,** 497 (1992).
7. J. F. de Haan, "Effects of aerosols on the brightness and polarization of cloudless planetary atmospheres," Ph.D. dissertation (Free University, Amsterdam, 1987).
8. W. J. Wiscombe and A. Mugnai, "Scattering from nonspherical Chebyshev particles. 2: means of angular scattering patterns," Appl. Opt. **27,** 2405–2421 (1988).
9. P. Stammes, "Light scattering properties of aerosols and the radiation inside a planetary atmosphere," Ph.D. dissertation (Free University, Amsterdam, 1989).
10. F. Kuik, J. F. de Haan, and J. W. Hovenier, "Single scattering of light by circular cylinders," Appl. Opt. **33,** 4906–4918 (1994).
11. W. M. F. Wauben, J. F. de Haan, and J. W. Hovenier, "Influence of particle shape on the polarized radiation in planetary atmospheres," J. Quant. Spectrosc. Radiat. Transfer **50,** 237–246 (1993).
12. H. C. van de Hulst, *Light Scattering by Small Particles* (Wiley, New York, 1957).
13. J. E. Hansen and L. D. Travis, "Light scattering in planetary atmospheres," Space Sci. Rev. **16,** 527–610 (1974).
14. C. F. Bohren and D. R. Huffman, *Absorption and Scattering of Light by Small Particles* (Wiley, New York, 1983).
15. F. Kuik, J. F. de Haan, and J. W. Hovenier, "Benchmark results for single scattering by spheroids," J. Quant. Spectrosc. Radiat. Transfer **47,** 477–489 (1992).
16. J. W. Hovenier and C. V. M. van der Mee, "Fundamental relationships relevant to the transfer of polarized light in a scattering atmosphere," Astron. Astrophys. **128,** 1–16 (1983).
17. J. F. de Haan, P. B. Bosma, and J. W. Hovenier, "The adding method for multiple scattering calculations of polarized light," Astron. Astrophys. **183,** 371–391 (1987).
18. I. M. Gelfand, R. A. Minlos, and Z. Y. Shapiro, *Representations of the Rotation and Lorentz Groups and Their Applications* (Pergamon, Oxford, 1963).
19. G. A. d'Almeida, P. Koepke, and E. P. Shettle, *Atmospheric Aerosols* (Deepak, Hampton, Va., 1991).
20. A. Mugnai and W. J. Wiscombe, "Scattering from nonspherical Chebyshev particles. 1: cross sections, single-scattering albedo, asymmetry factor, and backscattered fraction," Appl. Opt. **25,** 1235–1244 (1986).
21. M. I. Mishchenko, D. W. Mackowski, and L. D. Travis, "Scattering of light by bispheres with touching and separated components," Appl. Opt. **34,** 4589–4599 (1995).
22. L. Tsang, J. A. Kong, and R. T. Shin, *Theory of Microwave Remote Sensing* (Wiley, New York, 1985).
23. M. I. Mishchenko and L. D. Travis, "T-matrix computations of light scattering by large spheroidal particles," Opt. Commun. **109,** 16–21 (1994).
24. D. S. Saxon, "Tensor scattering matrix for the electromagnetic field," Phys. Rev. **100,** 1771–1775 (1955).
25. F. Kuik, "Single scattering of light by ensembles of particles with various shapes," Ph.D. dissertation (Free University, Amsterdam, 1992).
26. C. -R. Hu, G. W. Kattawar, M. E. Parkin, and P. Herb, "Symmetry theorems on the forward and backward scattering Mueller matrices for light scattering from a nonspherical dielectric scatterer," Appl. Opt. **26,** 4159–4173 (1987).

27. M. I. Mishchenko and J. W. Hovenier, "Depolarization of light backscattered by randomly oriented nonspherical particles," Opt. Lett. **20,** 1356–1358 (1995).
28. E. S. Fry and G. W. Kattawar, "Relationships between the elements of the Stokes matrix," Appl. Opt. **20,** 2811–2814 (1981).
29. J. W. Hovenier, H. C. van de Hulst, and C. V. M. van der Mee, "Conditions for the elements of the scattering matrix," Astron. Astrophys. **157,** 301–310 (1986).
30. C. V. M. van der Mee and J. W. Hovenier, "Expansion coefficients in polarized light transfer," Astron. Astrophys. **228,** 559–568 (1990).
31. A. Macke, M. I. Mishchenko, K. Muinonen, and B. E. Carlson, "Scattering of light by large nonspherical particles: ray tracing approximation versus *T*-matrix method," Opt. Lett. **20,** 1934–1936 (1995).
32. M. I. Mishchenko, "Reflection of polarized light by plane-parallel slabs containing randomly-oriented, nonspherical particles," J. Quant. Spectrosc. Radiat. Transfer **46,** 171–181 (1991).
33. M. I. Mishchenko and D. W. Mackowski, "Electromagnetic scattering by randomly oriented bispheres: comparison of theory and experiment and benchmark calculations," J. Quant. Spectrosc. Radiat. Transfer **55,** 683–694 (1996).
34. W. J. Wiscombe and G. W. Grams, "The backscattered fraction in two-stream approximations," J. Atmos. Sci. **33,** 2440–2451 (1976).
35. S. F. Marshall, D. S. Covert, and R. J. Charlson, "Relationship between asymmetry parameter and hemispheric backscatter ratio: implications for climate forcing by aerosols," Appl. Opt. **34,** 6306–6311 (1995).
36. M. I. Mishchenko, L. D. Travis, R. A. Kahn, and R. A. West, "Modeling phase functions for dust-like tropospheric aerosols using a shape mixture of randomly oriented polydisperse spheroids," submitted to J. Geophys. Res.
37. G. S. Kent, G. K. Yue, U. O. Farrukh, and A. Deepak, "Modeling atmospheric aerosol backscatter at CO_2 laser wavelengths. 1: aerosol properties, modeling techniques, and associated problems," Appl. Opt. **22,** 1655–1665 (1983).
38. Y. Sasano and E. V. Browell, "Light scattering characteristics of various aerosol types derived from multiple wavelength lidar observations," Appl. Opt. **28,** 1670–1679 (1989).
39. V. Srivastava, M. A. Jarzembski, and D. A. Bowdle, "Comparison of calculated aerosol backscatter at 9.1- and 2.1-μm wavelengths," Appl. Opt. **31,** 1904–1906 (1992).
40. G. L. Stephens, *Remote Sensing of the Lower Atmosphere* (Oxford U. Press, New York, 1994).
41. S. Asano and M. Sato, "Light scattering by randomly oriented spheroidal particles," Appl. Opt. **19,** 962–974 (1980).
42. R. J. Perry, A. J. Hunt, and D. R. Huffman, "Experimental determinations of Mueller scattering matrices for nonspherical particles," Appl. Opt. **17,** 2700–2710 (1978).
43. K. Sassen and K. -N. Liou, "Scattering of polarized laser light by water droplet, mixed-phase and ice-crystal clouds. Part I: angular scattering patterns," J. Atmos. Sci. **36,** 838–851 (1979).
44. M. I. Mishchenko, "Light scattering by nonspherical ice grains: an application to noctilucent cloud particles," Earth Moon Planets **57,** 203–211 (1992).
45. K. Sassen, "The polarization radar technique for cloud research: a review and current assessment," Bull. Am. Meteorol. Soc. **72,** 1848–1866 (1991).
46. W. L. Eberhard, "Ice-cloud depolarization of backscatter for CO_2 and other infrared lidars," Appl. Opt. **31,** 6485–6490 (1992).
47. S. J. Ostro, "Planetary radar astronomy," Rev. Mod. Phys. **65,** 1235–1279 (1993).
48. L. Stefanutti, M. Morandi, M. Del Guasta, S. Godin, and C. David, "Unusual PSCs observed by LIDAR in Antarctica," Geophys. Res. Lett. **22,** 2377–2380 (1995).
49. R. H. Zerull, "Scattering measurements of dielectric and absorbing nonspherical particles," Contrib. Atmos. Phys./Beitr. Phys. Atmos. **49,** 168–188 (1976).
50. K. -N. Liou and H. Lahore, "Laser sensing of cloud composition: a backscattered depolarization technique," J. Appl. Meteorol. **13,** 257–263 (1974).
51. M. I. Mishchenko, A. A. Lacis, B. E. Carlson, and L. D. Travis, "Nonsphericity of dust-like tropospheric aerosols: implications for aerosol remote sensing and climate modeling," Geophys. Res. Lett. **22,** 1077–1080 (1995).